cond-mat/9707290 McGill-97/11, UdeM-GPP-TH-97-41

A Microscopic Derivation of the SO(5)-Symmetric Landau-Ginzburg Potential

C.P. Burgess[a], J.M. Cline[a], R. MacKenzie[b] and R. Ray[b]

[a] *Physics Department, McGill University*

3600 University St., Montréal, Québec, Canada, H3A 2T8.

[b] *Laboratoire René-J.-A.-Lévesque, Université de Montréal*

C.P. 6128, Succ. centre-ville, Montréal, Québec, Canada, H3C 3J7.

Abstract

We construct a microscopic model of electron interactions which gives rise to both superconductivity and antiferromagnetism, and which admits an approximate $SO(5)$ symmetry that relates these two phases. The symmetry can be exact, or it may exist only in the long-wavelength limit, depending on the detailed form of the interactions. We compute the macroscopic Landau-Ginzburg free energy for this model as a function of temperature and doping, by explicitly integrating out the fermions. We find that the resulting phase diagram can resemble that observed for the cuprates, with the antiferromagnetism realized as a spin density wave, whose wavelength might be incommensurate with the lattice spacing away from half filling.

1. Introduction and Summary

Zhang has recently proposed [1] that the superconducting and antiferromagnetic phases of the high-T_c cuprates might be related to one another by an approximate $SO(5)$ symmetry of the electronic Hubbard Hamiltonian. This proposal incorporates in a fundamental way the connection between antiferromagnetism (AF) and superconductivity (SC) which is observed in these systems.

Recently, however, the foundations of this picture have come under attack, with criticism directed against the existence of an approximate $SO(5)$ symmetry of the Hubbard Hamiltonian [2] (for a reply, see [3]), as well as against the very possibility, in principle, of relating the antiferromagnetic and superconducting phases by the rotation of a finite-dimensional order parameter [4]. This motivates studying whether and under what conditions an approximate $SO(5)$ symmetry can emerge from a microscopic picture of electron dynamics.

In this paper we investigate a model of electron dynamics which can naturally incorporate an approximate $SO(5)$ symmetry.[1] Our model consists of degenerate electrons with two kinds of attractive interactions, described by a four-Fermi Hamiltonian of the form $H = H_0 + H_{\rm int}$, where $H_{\rm int} = H_{AF} + H_{SC}$, and

$$H_0 = \sum_p \left(\varepsilon_p - \mu\right)\, \psi_p^\dagger \psi_p + \sum_q \Big(a_\phi^0\, \phi_q^* \phi_q + a_n^0\, \vec{n}_q^{\,*} \cdot \vec{n}_q \Big), \tag{1}$$

$$H_{AF} = \frac{1}{2V} \sum_{pq} f(p,q)\, \Big(\psi_{p+Q+q}^\dagger \vec{\sigma}\, \psi_p \Big) \cdot \vec{n}_{Q+q} + \text{h.c.}, \tag{2}$$

$$H_{SC} = \frac{1}{2V} \sum_{pq} g(p,q)\, \Big(\psi_{-p-q}^T \sigma_2\, \psi_p \Big) \phi_q + \text{h.c.}, \tag{3}$$

Here $\psi_p = \begin{pmatrix} \psi_{p\uparrow} \\ \psi_{p\downarrow} \end{pmatrix}$ is the electron field, while ϕ_q and $\vec{n}_q$ are Hubbard-Stratonovich auxiliary scalar fields which, when integrated out, produce the two four-Fermi interactions. ε_p denotes the electron single-particle dispersion relation, μ is the chemical potential that measures deviations from half-filling, and $\vec{\sigma} = \{\sigma_i, i = 1,2,3\}$ are the Pauli matrices. Q is

[1] A broader class of similar models has recently been proposed in ref. [5].

a fixed nesting vector which will be defined below. a_ϕ^0 and a_n^0 are positive constants which could, if one wished, be absorbed into the definitions of f and g by a redefinition of ϕ and $\vec{n}$; however it is convenient to keep them for the purposes of renormalization in §4.

Our goal in this work is twofold: first, to find the conditions under which this model exhibits an approximate $SO(5)$ symmetry, and to see how the symmetry-breaking effects manifest themselves at temperatures much less than the Fermi energy. We find the symmetry to be possible, and it can arise "accidentally"at long wavelengths even if it is not important for the microscopic dynamics. We also find that symmetry-breaking effects are marginal, for weak couplings, in the sense that they increase only logarithmically as one scales into the infrared. Second, we wish to compute the effective Landau-Ginzburg (LG) potential, so as to determine how the phase diagram depends on the microscopic electronic couplings. The result is that the AF phase can have the phenomenologically desired shape in the temperature-doping plane, preferring low temperatures and zero doping. Moreover the SC phase, while also preferring small doping, is not suppressed as quickly by increased doping as is the AF phase. The result is that SC becomes energetically favorable to AF at some lower critical doping, and persists until some upper critical doping. These results are consistent with but more predictive than the general effective-field-theory description of [1] and [6]. For example they predict the absence of a mixed AF/SC phase away from zero doping when the fundamental Hamiltonian is $SO(5)$-invariant. They also agree with the observed phase diagram of the high-T_c systems, although we do not attempt here a detailed discussion of the applicability of these models to the cuprates.

Our analysis of the model defined by eqs. (1)–(3) is motivated by the renormalization-group (RG) approach to understanding superconductivity and antiferromagnetism as BCS and spin-density-wave instabilities within Fermi liquid theory [7]. In the RG language, a Fermi liquid is understood as a regime of scales for which the dominant quasiparticle degrees of freedom are weakly-coupled, degenerate fermions carrying the same quantum numbers as the underlying electrons. Under such circumstances almost all of the quasiparticle self-interactions are irrelevant in the RG sense: they become less and less important as one integrates out high energy modes to obtain an effective Hamiltonian valid near the

Fermi surface.

The only exceptions to the rule that interactions are irrelevant in the infrared are certain four-Fermi terms, which can be marginally relevant for special kinds of electron kinematics. An important example is any pairwise attraction between electrons (or holes) having opposite momenta. This kind of interaction grows logarithmically in the infrared, eventually becoming strong enough to trigger the BCS instability at sufficiently low energies. A second exception exists when the quasiparticle Fermi surface (FS) is nested.[2] In this case the attraction between electrons whose momenta sum to the nesting vector, Q, is also marginally relevant, potentially triggering an instability towards the formation of a condensate which is modulated in space with wavevector Q. The result is a charge- or spin-density wave depending on the electric charge and spin of the attractive channel.

We have both types of instability in mind when using the Hamiltonian in eqs. (1)–(3). It is assumed that the quasiparticle energies ε_p are time-reversal invariant, $\varepsilon_{-p} = \varepsilon_p$, and have a FS with a nesting vector Q, defined by the property $\varepsilon_{p+Q} = -\varepsilon_p$ for p near the FS. (Our convention is to define the FS at half filling to be the zero of energy.) An example of a dispersion relation with these properties in two dimensions is that of the extended Hubbard model,

$$\varepsilon_p = -2t\Big[\cos(p_x a) + \cos(p_y a)\Big], \tag{4}$$

where a is the lattice spacing and the nesting vector is $Q = \big(\pm\frac{\pi}{a}, \pm\frac{\pi}{a}\big)$. However the general analysis that follows in §4 does not depend on using this explicit form. Notice that because antiferromagnetism arises here as a spin-density wave, its periodicity need not be precisely commensurate with the lattice spacing, particularly away from half filling. Such incommensurate antiferromagnetism is particularly interesting in view of the splitting of the AF peaks which is seen in recent neutron-scattering data [8].

Since eqs. (1)–(3) involve an attractive interaction in the spin-triplet channel, the nesting produces a spin-density-wave instability. The Hubbard-Stratonovich formulation of the Hamiltonian, eqs. (1)–(3), is particularly convenient for following these instabilities of the

[2] The FS is nested if its opposite edges are related to one another by a fixed tranlation, Q, in momentum space.

system since they may be studied by examining the minima of the potential for the modes ϕ_0 and $\vec{n}_Q$, which is induced when the electrons are integrated out. Depending on which of these modes condenses most strongly, the resulting ordered phases are superconductors or antiferromagnets, possibly both.

Our presentation is organized as follows. In the next section, §2, the conditions for the Hamiltonian, eqs. (1)–(3), to exhibit $SO(5)$ symmetry are derived. We find that the symmetry is present in the long-wavelength limit, $q \to 0$, if the coupling functions satisfy the relation $f^2 = g^2$. In §3 we integrate out the electrons to obtain the long-wavelength effective potential for the order parameters, ϕ_0 and $\vec{n}_Q$. The expressions obtained in §3 are evaluated in §4, in the limit of degenerate electrons, *i.e.* with all couplings and dispersion relations linearized around the FS. We present explicit expressions in this limit for the coefficients of the Landau-Ginzburg theory, as functions of the fundamental fermion couplings, temperature and chemical potential. In some parts of the phase diagram the usual expansion of the free energy to quartic order in the fields is unbounded from below, forcing us to use the full potential. From these results it is straightforward to determine the main features of the phase diagram. We find the dependence on T and μ can have the desired form if the AF interaction in eq. (2) is chosen to be somewhat ($\sim 10 - 20\%$) stronger than the SC interaction of eq. (3). In §5 we examine the validity of the degenerate-electron approximation by recomputing the quadratic and quartic terms of the effective potential without linearizing about the FS. We do so using specific choices of ε, f and g that have been previously suggested [1,5,9] in connection with d-wave superconductivity, to show that the approximations used in §4 are indeed reliable. §6 concludes with a brief recapitulation of our results.

2. The $SO(5)$ Symmetry

In this section we identify the conditions under which the Hamiltonian, eqs. (1)–(3), admits an $SO(5)$ symmetry along the lines Zhang has proposed.

2.1) The Algebra

$SO(5)$ symmetry contains as a subgroup the $SO(3) \times SO(2)$ group of spin rotations and electromagnetic gauge transformations, with respect to which H is obviously invariant. The electron part of the corresponding conserved charges (electric charge and spin) are given by:

$$\mathcal{Q} = \sum_p \psi_p^\dagger \, \psi_p, \qquad \text{and} \qquad \vec{S} = \frac{1}{2} \sum_p \psi_p^\dagger \vec{\sigma} \psi_p. \tag{5}$$

The nontrivial requirement for $SO(5)$ invariance is the existence of the electrically-charged, spin-triplet off-diagonal operators, $\vec{\Pi}$, whose real and imaginary parts fill out the generators of $SO(5)$ in addition to $\mathcal{Q}$ and $\vec{S}$. Motivated by Zhang's [1] choice, we take its action on electrons to be given by

$$\vec{\Pi} \equiv \sum_p h_p \, (\psi^T_{-p+Q} \sigma_2 \, \vec{\sigma} \, \psi_p), \tag{6}$$

where h_p is a function to be determined. As is easily verified, this has the desired commutation relations with $\mathcal{Q}$ and $\vec{S}$, and satisfies $\Big[\Pi_a, \Pi_b\Big] = 0$. In addition, if the function h_p shares the same properties as does ε_p: *i.e.* $h_{p+Q} = -h_p$, and $h_{-p} = h_p$, then:

$$\Big[\Pi_a, \Pi_b^*\Big] = 4 \sum_p \, |h_p|^2 \left[(\psi_p^\dagger \, \psi_p) \, \delta_{ab} - i \epsilon_{abc} \, (\psi_p^\dagger \, \sigma_c \, \psi_p) \right]. \tag{7}$$

Eq. (7) shows that $\{\mathcal{Q}, \vec{S}, \vec{\Pi}, \vec{\Pi}^*\}$ satisfy the $SO(5)$ commutation relations provided we choose $|h_p| = c$, where c is an appropriately chosen constant. This is only consistent with the property $h_{p+Q} = -h_p$ if $h_p = \pm c$ for p inside the FS, and $h_p = \mp c$ outside.

2.2) Conditions for Symmetry

We next determine the conditions under which the Hamiltonian, eqs. (1)–(3), commutes with the $\vec{\Pi}$. A nonvanishing chemical potential explicitly breaks $SO(5)$ down to $SO(3) \times SO(2)$, so we set $\mu = 0$ here. Furthermore, we ignore for now the scalar part of H_0, which is invariant provided ϕ and $\vec{n}$ transform together in the fundamental representation of $SO(5)$. The electron part of the free Hamiltonian then satisfies:

$$\Big[\Pi_a, H_0^{el}\Big] = -2 \sum_p \varepsilon_p \, h_p \, (\psi^T_{Q-p} \, \sigma_2 \sigma_a \, \psi_p). \tag{8}$$

This vanishes by virtue of the Fermi statistics of ψ, provided that ε_p shares the previously advertised symmetry properties of h_p: *i.e.* if $\varepsilon_{p+Q} = -\varepsilon_p$ and $\varepsilon_{-p} = \varepsilon_p$.

For notational convenience, we define the operators appearing in $H_{\rm int}$ by $V_b(q)$ and $W(q)$, where $V_b(q) \equiv \sum_p f(p,q) \; (\psi^\dagger_{p+q+Q} \, \sigma_b \, \psi_p)$, and $W(q) \equiv \sum_p g(p,q) \, (\psi^\dagger_{-p+q} \, \sigma_2 \, \psi^*_p)$. Then

$$\begin{aligned}
\Big[\Pi_a, W^*(q)\Big] &= 2 \sum_p \Big[g^*(p+q-Q,q) + g^*(Q-p,q)\Big] \, h_p \; (\psi^\dagger_{p-Q+q} \, \sigma_a \, \psi_p), \\
\Big[\Pi_a, V_b(q)\Big] &= 2 \sum_p f(p,q) \, h_{p+q} \; (\psi^T_{-p-q} \, \sigma_2 \, \sigma_a \sigma_b \, \psi_p) \\
&= \sum_p \Big[f(p,q) \, h_{p+q} + f(-p-q,q) \, h_{-p}\Big] \; (\psi^T_{-p-q} \, \sigma_2 \, \psi_p) \\
&\qquad + i\epsilon_{abc} \sum_p \Big[f(p,q) \, h_{p+q} - f(-p-q,q) \, h_{-p}\Big] \; (\psi^T_{-p-q} \, \sigma_2 \, \sigma_c \, \psi_p).
\end{aligned} \tag{9}$$

The operators V_a and W rotate into one another as a five-dimensional vector of $SO(5)$ provided the coupling functions satisfy the conditions $f(p,q) \, h_{p+q} \equiv f(-p-q,q) \, h_{-p} \propto g^*(p,q)$ and $[g^*(p+q-Q,q) + g^*(Q-p,q)]h_p \propto f(p,q)$.

Of particular interest for many purposes, particularly the phase diagram, is the long-wavelength limit, $q \to 0$. In this limit we have $\Big[\Pi_a, V_b(0)\Big] = -4\delta_{ab} \, W^*(0)$ and $\Big[\Pi_a, W(0)\Big] = -4 \; V_a(0)$, provided the functions $f_p \equiv \lim_{q\to 0} f(p,q)$ and $g_p \equiv \lim_{q\to 0} g(p,q)$ satisfy the properties $f_p = f_{-p}$, $g_p = g_{-p} = -g_{p+Q}$ and $f_p h_p = g_p$ and $g_p h_p = f_p$. Given

our earlier choice that $h_p = \pm c$, with opposite signs inside and outside the FS, we see that $W(0)$ and $V_b(0)$ fill out the fundamental representation of $SO(5)$ provided that the coupling functions satisfy $f_p = \mathrm{sign}(\varepsilon_p) g_p$.

Finally, so long as W and V_b transform as a **5** of $SO(5)$, the entire Hamiltonian, eqs. (1)–(3), is $SO(5)$ invariant, provided that $SO(5)$ is taken also to rotate the five scalars, $\mathrm{Re}(\phi_0)/\sqrt{2}$, $\mathrm{Im}(\phi_0)/\sqrt{2}$ and $\vec{n}_Q$, into one another as a **5**. Notice that although the demands made on f and g for exact $SO(5)$ symmetry are quite strong, the symmetry can emerge for small q under much weaker conditions, and this is sufficient for the invariance of the phase diagram.

3. Integrating out the Electrons

We now turn to the derivation of the effective theory which governs the long-wavelength scalar modes, ϕ_0 and $\vec{n}_Q$. The resulting effective potential will be subsequently used to identify the phase diagram of the system, and to see to what extent it exhibits $SO(5)$ invariance. Since the effective potential must be symmetric under $U(1)$ transformations of ϕ_0 and under $SO(3)$ rotations of $\vec{n}_Q$, for notational simplicity we shall take $\phi_0 \equiv \phi$ real and $(n_Q)_i = n\,\delta_{i,3}$.

3.1) Preliminary Issues

The thermodynamic variables we wish to follow in the LG potential are the values of the fields ϕ and n themselves, as well as the temperature, T, and the electron doping away from half-filling, x. We therefore ignore all scalar modes apart from ϕ and n, and compute the effective potential for these variables. In order to follow the doping we also introduce a chemical potential, μ, which measures the change in density away from the free-particle FS (which is defined here by $\varepsilon_p = 0$).

We now integrate out the electrons, using the Hamiltonian, eqs. (1)–(3), supplemented by the chemical potential. To incorporate the Fermi sea we exchange the electron field, ψ_p for p inside the FS, for a hole field, $\chi_p = \sigma_2\, \psi^*_{-p}$, in the usual way, permitting the use of vacuum propagators for the integration over the fermion fields.

For the purposes of performing the functional integral over ψ_p and χ_p, it is convenient to group ψ_p, ψ_p^* and their counterparts having momentum $-p$ and $p-Q$ into the following 16-component vector:

$$\Psi_p \equiv \begin{pmatrix} \psi_p \\ \psi_p^* \\ \psi_{p-Q} \\ \psi_{p-Q}^* \\ \psi_{-p} \\ \psi_{-p}^* \\ \psi_{Q-p} \\ \psi_{Q-p}^* \end{pmatrix} = \begin{pmatrix} \psi_p \\ \psi_p^* \\ \sigma_2\, \chi_{Q-p}^* \\ \sigma_2\, \chi_{Q-p} \\ \psi_{-p} \\ \psi_{-p}^* \\ \sigma_2\, \chi_{p-Q}^* \\ \sigma_2\, \chi_{p-Q} \end{pmatrix}. \tag{10}$$

When Ψ_p is used as the field, all sums over p must be restricted to the original Brillouin zone, modulo the transformations $p \to -p$ and $p \to p+Q$.

With this choice the quadratic part of the Hamiltonian may be written $\frac{1}{2}\, \Psi_p^\dagger\, \Delta\, \Psi_p$, with:

$$\Delta \equiv \begin{pmatrix} A & B \\ B & A \end{pmatrix}, \tag{11}$$

and A and B denoting the following 8×8 matrices:

$$A = \begin{pmatrix} \varepsilon_p - \mu & 0 & f_p n\, \sigma_3 & 0 \\ 0 & -\varepsilon_p + \mu & 0 & f_p n\, \sigma_3 \\ f_p n\, \sigma_3 & 0 & -\varepsilon_p - \mu & 0 \\ 0 & f_p n\, \sigma_3 & 0 & \varepsilon_p + \mu \end{pmatrix}, \tag{12}$$

and

$$B = \begin{pmatrix} 0 & g_p \phi\, \sigma_2 & 0 & 0 \\ g_p \phi\, \sigma_2 & 0 & 0 & 0 \\ 0 & 0 & 0 & g_p \phi\, \sigma_2 \\ 0 & 0 & g_p \phi\, \sigma_2 & 0 \end{pmatrix}. \tag{13}$$

In these last expressions, each entry of the matrices A and B are 2×2 matrices in spin space.

3.2) The Functional Determinant

Standard methods may now be used to compute the functional integral over the fermion fields. Using the matrix form for the Hamiltonian, eqs. (11)–(13), the result

for the one-loop, finite-temperature contribution to the free energy density, F_1, in d spatial dimensions is:

$$\begin{aligned} -\beta F_1(\phi, n) &= \frac{1}{2} \ln \det \Big[-\partial_t^2 + \Delta^2 \Big] \\ &= \frac{1}{2} \int \frac{d^d p}{(2\pi)^d} \sum_{j=-\infty}^{\infty} \Big[\ln\Big(\omega_j^2 + \lambda_+^2 \Big) + \ln\Big(\omega_j^2 + \lambda_-^2 \Big) \Big], \\ &= \int \frac{d^d p}{(2\pi)^d} \, \ln \left[\cosh\left(\beta \, \lambda_+/2\right) \cosh\left(\beta \, \lambda_-/2\right) \right], \end{aligned} \tag{14}$$

where, as usual, $\beta = 1/kT$ and the sum is over the Matsubara frequencies, $\omega_j = (2j+1)\pi\beta$. We have switched to continuum momenta, and restored the integration region to the full Brillouin zone (so that it is no longer modded out by $p \to -p$ and $p \to p + Q$). The eigenvalues of the Hamiltonian Δ are given by

$$\lambda_\pm = \left[\left(\sqrt{\varepsilon_p^2 + (f_p n)^2} \pm \mu \right)^2 + (g_p \phi)^2 \right]^{\frac{1}{2}}. \tag{15}$$

Even before undertaking a detailed evaluation of the free energy (14), we can prove an interesting result: in the $SO(5)$ limit where $f_p^2/a_n^0 = g_p^2/a_\phi^0$, and for nonzero doping, $\mu \neq 0$, the ground state must have $\phi = 0$ or $n = 0$ (possibly both) and hence is never a mixed phase of AF and SC. This follows from the form of the energy eigenvalues (15) in the conditions for minimizing the free energy. Adding F_1 to the tree-level free energy $F_0 = a_\phi^0 \phi^2 + a_n^0 n^2$, these conditions are

$$\frac{1}{2} \frac{\partial F}{\partial X} = a_X^0 X - \frac{1}{2} \int \frac{d^d p}{(2\pi)^d} \sum_\pm \tanh\left(\beta \, \lambda_\pm/2\right) \frac{\partial \lambda_\pm}{\partial X} \tag{16}$$

where X stands for either of the fields ϕ or n. The derivatives of the eigenvalues have the form

$$\frac{\partial \lambda_\pm}{\partial \phi} = \frac{g_p^2 \phi}{\lambda_\pm}; \qquad \frac{\partial \lambda_\pm}{\partial n} = \frac{f_p^2 n}{\lambda_\pm} \left(1 \pm \frac{\mu}{\sqrt{\varepsilon_p^2 + (f_p n)^2}} \right) \tag{17}$$

When $f_p^2 = g_p^2$ and $a_\phi^0 = a_n^0 = a^0$, the minimization conditions can be written in the form

$$\frac{1}{2} \frac{\partial F}{\partial \phi} = \phi (a^0 - G), \qquad \frac{1}{2} \frac{\partial F}{\partial n} = n (a^0 - G + \mu^2 H), \tag{18}$$

where it is easily shown that G and μH are positive definite functions. Therefore in this limit there are never simultaneous solutions where both ϕ and n are nonvanishing, except when μ vanishes.

When evaluating these expressions in the next section, we focus on the degenerate limit, for which kT is much less than the Fermi energy at zero doping. For example, using the explicit dispersion relation given by eq. (4), this corresponds to neglecting powers of kT/t. In this limit only states near the Fermi surface are important in the integrals, and it is useful to decompose the momentum p into a component k on the FS and a component ℓ perpendicular to the FS. We may then linearize all quantities in ℓ, restrict the coupling functions g and f to momenta lying in the FS, and obtain for the dispersion relation $\varepsilon \approx v_{_F}\ell$, with the Fermi velocity, $v_{_F}(k)$, generally being a function of momentum, k.

Eqs. (14) and (15) are this section's main results. We now extract their implications for the LG potential,[3] first by examining them in detail in the vicinity of zero fields, $\phi = n = 0$, and then by computing the potential for arbitrarily values of the fields, in certain directions in the ϕ-n plane.

4. The Landau-Ginzburg Theory

Eqs. (14) and (15) define the effective potential for the SC order parameter, ϕ, and the AF order parameter, n. Since this potential is analytic[4] at $\phi = n = 0$, an expansion to quartic order in the fields gives a good indication of when a condensate will form for either ϕ or n. However we will find that the quartic terms do not always stabilize the potential, and it is necessary to know how the full potential looks away from $\phi = n = 0$. In this case we will use the full free energy in order to determine the phase diagram of the system.

[3] See refs. [9] for related calculations of the LG free energy for high-T_c systems.

[4] The same is not true of the zero-temperature limit of the potential, which has the nonanalytic behavior $\phi^2 \ln \phi^2$ in the vicinity of ϕ=0.

4.1) Analytic Expressions in the Quartic Approximation

We start by approximating the free energy with a quartic potential, whose form we take to be

$$\beta[F - F(0)] = \Big(a_\phi\,\phi^2 + a_n n^2\Big) + \frac{1}{4}\Big(b_{\phi\phi}\phi^4 + 2\,b_{\phi n}\phi^2 n^2 + b_{nn}n^4\Big) + \cdots \tag{19}$$

where the ellipsis denotes terms involving more than four powers of ϕ or n. Using Eqs. (14) and (15) and defining

$$N_{n,m} = \frac{1}{2\hbar^{d-1}}\int \frac{d^{d-1}k\; f^n\, g^m}{(2\pi)^d v_{_F}(k)}, \qquad \xi = \varepsilon - \mu\,, \qquad T_\beta(\xi) = \frac{\tanh(\beta\xi/2)}{\xi}, \tag{20}$$

we find that the quadratic coefficients are given by the following integrals:

$$a_\phi = a_\phi^0(\Lambda) - N_{0,2}\int_{-\Lambda}^{\Lambda} d\varepsilon\; T_\beta(\xi), \tag{21}$$

$$a_n = a_n^0(\Lambda) - N_{2,0}\int_{-\Lambda}^{\Lambda} d\varepsilon\; T_\beta(\xi)\frac{\xi}{\varepsilon}, \tag{22}$$

where a_ϕ^0 and a_n^0 are the "bare" values of these quantities that appear in the original Hamiltonian, eqs. (1)–(3). The integral over ε diverges logarithmically in the ultraviolet, forcing the introduction of the cutoff scale, Λ. Physically this scale represents the energies for which the linearization of the quasiparticle spectrum no longer applies, or where the degrees of freedom of the Hamiltonian, eqs. (1)–(3), are no longer appropriate, whichever is lower. If these approximations were exact, then Λ would be the actual maximum energy available on the lattice. In any case, we can consider Λ to be of order the Fermi energy. The divergent dependence on Λ as $\Lambda \to \infty$ can be absorbed into a renormalization of a_ϕ^0 and a_n^0.

The quartic coefficients are given similarly by the following expressions, which since they are convergent allow us to take the cutoff Λ to infinity if we wish:

$$b_{\phi\phi} = -\;N_{0,4}\;\int_{-\Lambda}^{\Lambda} d\varepsilon\,\frac{T'_\beta(\xi)}{\xi}, \tag{23}$$

$$b_{\phi n} = -\ N_{2,2} \int_{-\Lambda}^{\Lambda} d\varepsilon\, \frac{T'_\beta(\xi)}{\varepsilon}, \tag{24}$$

$$b_{nn} = -\ N_{4,0} \int_{-\Lambda}^{\Lambda} d\varepsilon\, \left(\frac{T'_\beta(\xi)}{\varepsilon} - \frac{\mu}{\varepsilon} \frac{\partial}{\partial \varepsilon} \left(\frac{T_\beta(\xi)}{\varepsilon} \right) \right). \tag{25}$$

The approximation $\Lambda \to \infty$ is only valid if T and μ are much smaller than the Fermi energy.

Because we work in the degenerate limit, near the FS, and at zero field, the shape of the coefficient functions as k varies over the FS enters only as an overall normalization factor. As expected from our previous discussion, the $SO(5)$ symmetry is manisfestly present in the limit $\mu = 0$ and $f^2/a_n^0 = g^2/a_\phi^0$.

4.2) Instability Towards Condensation

Before turning to the numerical evaluation of these integrals, it is instructive to first explore the physical implications of the renormalization itself. Because the sign of the loop contributions to a_ϕ and a_n is negative, these quantities decrease as the temperature is decreased. In the limit of large $\beta\Lambda$, it is easy to see that the one-loop contributions $\Delta a_X = a_X - a_X^0$ have the limiting behavior

$$\Delta a_\phi \sim -2\, N_{0,2} \ln(\beta\Lambda); \qquad \Delta a_n \sim -2\, N_{2,0} \ln(\beta\Lambda). \tag{26}$$

Even if $a_\phi(T \sim \Lambda)$ and $a_n(T \sim \Lambda)$ are initially chosen to be positive, so that F is minimized by $\phi = n = 0$, eventually their decrease with decreasing T can drive them negative, causing an instability towards the development of nonzero condenstates for ϕ or n.

Eq. (26) gives the evolution of the $SO(5)$-breaking combination of the electron couplings:

$$\beta \frac{\partial}{\partial \beta}(a_\phi - a_n) = 2(N_{2,0} - N_{0,2}) = 2 \int \frac{d^{d-1}k}{(2\pi)^d v_F}\, (f^2 - g^2). \tag{27}$$

This shows that any $SO(5)$ breaking present in the original Hamiltonian due to $f^2 \neq g^2$ will be enhanced in the effective GL Hamiltonian by a potentially large logarithm of the

form $\ln(\beta\Lambda)$, where Λ is of the order of the Fermi energy. For example, suppose the AF pairing is taken to be s-wave, $f = f_0$, whereas the SC pairing is d-wave, corresponding to $g = g_0(\cos(ak_x) - \cos(ak_y))$. Here f_0 and g_0 are arbitrary constants. In general $N_{2,0}$ and $N_{0,2}$ differ from each other, and although g_0/f_0 can be tuned to make the difference vanish, there seems to be no symmetry principle that would require it to take this special value. Moreover, even if such a choice were made, it would still not insure that the quartic couplings would have $SO(5)$ symmetry, *i.e.*, $N_{4,0} = N_{0,4} = N_{2,2}$. In §5 we will say more about the extent of $SO(5)$-breaking that arises from this choice of coupling functions.

4.3) Numerical Results near $\phi = n = 0$

Figures (1) and (3) present plots of the coefficients of the potential as functions of the chemical potential, factoring out the integrals over the FS. In this section we describe these plots in more detail, and use them to deduce the general shape of the phase diagram in the temperature-doping plane.

Figure (1) plots the one-loop contribution to the quadratic coefficients in the dimensionless form $(a_n - a_n^0)/N_{0,2}$ and $(a_\phi - a_\phi^0)/N_{2,0}$, where $N_{n,m}$ are the FS integrals defined in (20). At zero doping these functions are negative and are increasing with temperature like $\ln(T/\Lambda)$, so it is always possible to choose the bare coefficients a_n^0 or a_ϕ^0 in such a way that a_n or a_ϕ is positive for high temperatures and changes sign at some T_c, triggering the instability toward condensation. As the doping is increased, a_n increases much more rapidly than a_ϕ. It follows that if the AF phase is energetically preferable to the SC phase at $\mu = 0$, the system will be AF at zero doping, and then make the transition to SC at some small doping, provided that a_ϕ is still negative at this value of μ.

With applications to the high-T_c cuprates in mind, we imagine $\Lambda \sim 0.1$ eV $\sim 10^3 K$ and so we adjust the bare coupling a_n^0 to ensure that the AF transition (Néel) temperature, T_N, at $\mu = 0$ is 1/10 of the cutoff scale, $\beta_N \Lambda = 10$. From fig. 1 it can be seen that at a temperature $T = T_N/10$, for example, we have $\beta\Lambda = 100$ and so the AF phase is quenched at a critical doping of $x_c \sim \mu_c/\Lambda = 10\,\%$. This is the doping at which $a_n(\mu_c)_{\beta\Lambda=100}$ becomes equal to $a_n(0)_{\beta\Lambda=10}$.

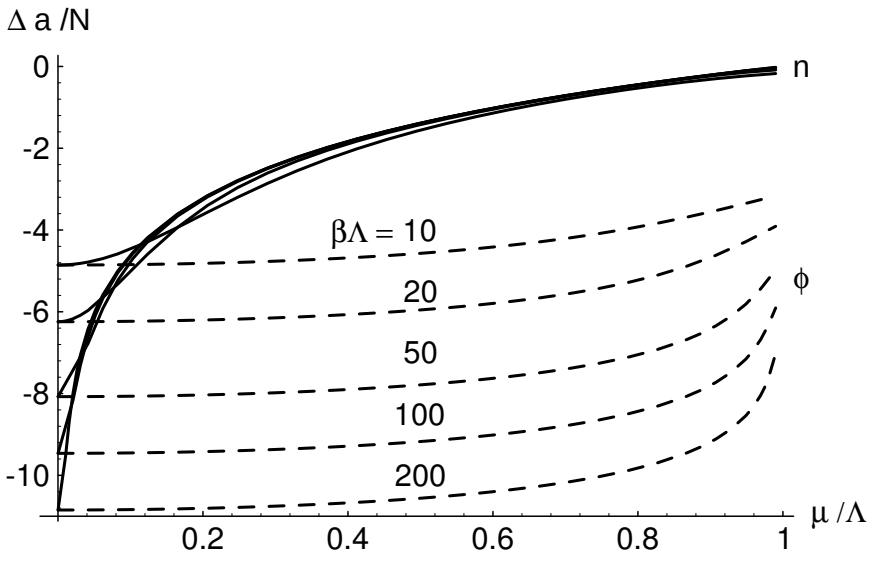

Figure 1

The coefficients $(a_\phi - a_\phi^0)/N_{0,2}$ (dashed) and $(a_n - a_n^0)/N_{2,0}$ (solid) as a function of μ/Λ, for $\beta\Lambda$=10, 20, 50, 100 and 200.

The above example ignores the SC order parameter, which would be valid if a_ϕ^0 was taken to be much larger than a_n^0. If on the other hand $SO(5)$ symmetry was realized, so that $a_\phi^0 = a_n^0$ and $N_{0,2} = N_{2,0}$, then at $\mu = 0$ the ground state would be an arbitrary admixture of AF and SC phases since both have the same energy. In this case, the system will always make a transition to the pure SC phase at the critical doping x_c. Since experiments indicate that at $\mu = 0$ the cuprates are pure AF, the SC phase must be suppressed by having $a_\phi^0/N_{0,2} > a_n^0/N_{2,0}$, so that SC is energetically disfavored until the critical doping is reached. In this situation, the phase diagram must have a form similar to figure 2. Of course, this prediction does not take account of quantum fluctuations within the effective theory itself. Such higher-loop effects are believed to be especially important near the bicritical point, where the SC phase first emerges [1]. They may have the effect of driving this point downward, leaving a gap between the SC and AF phases at temperatures somewhat above the existence of the bicritical point.

To determine exactly how much $SO(5)$ breaking is needed in the quadratic terms in order to suppress SC at zero doping, one must compare the local minima of the potential along the $\phi = 0$ and $n = 0$ axes and insure that the minimum with $n \neq 0$ is the deeper of the two. This issue can usually be settled by looking at the higher order terms in the

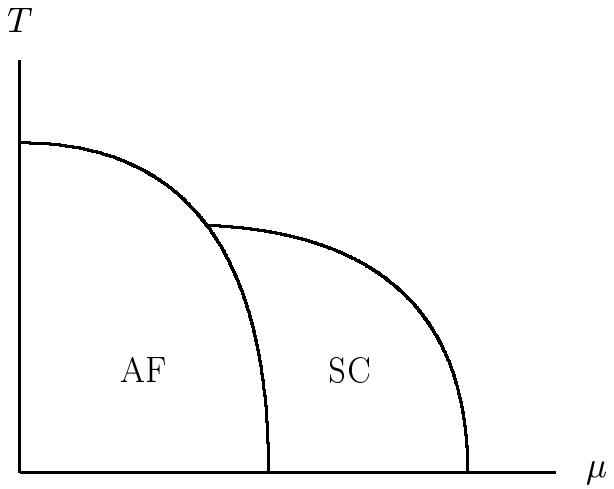

Figure 2

Schematic representation of the phase diagram for the present Hamiltonian, with $SO(5)$ symmetry broken to favor the AF condensate. Quantum effects not considered here may be able to drive the bicritical point downward.

potential. To this end we have computed the quartic coefficients in the dimensionless forms $b_{\phi\phi}T^2/N_{0,4}$, $b_{nn}T^2/N_{4,0}$ and $b_{n\phi}T^2/N_{2,2}$, and plotted them in fig. 3.

The fact that $b_{\phi\phi}$ is only weakly dependent on the doping can be see by observing that when $\Lambda \to \infty$, μ can be completely removed by shifting the integration variable from ε to ξ. The low temperature form of the quartic couplings can be further understood analytically through the identities

$$\lim_{\beta\to\infty} \frac{T'_\beta(\xi)}{\beta^2\,\xi} = -\frac{7\zeta(3)}{2\pi^2}\delta(\xi) \tag{28}$$

$$\lim_{\beta\to\infty} \frac{1}{\beta^2}\left[\frac{T'_\beta(\xi)\mu^2}{\xi\varepsilon^2} - \frac{\mu T_\beta(\xi)}{\varepsilon^3}\right] = -\frac{7\zeta(3)}{2\pi^2}\delta(\xi) \tag{29}$$

Eq. (29) is valid so long as it is combined with a function that is nonsingular at $\varepsilon = 0$, in which case its own $1/\varepsilon$ singularity can be integrated over using the principal value. Both of these representations of the delta function can break down if multiplied by singular functions of ξ, which is precisely what happens at $\mu = 0$, but for $\mu \gg 1/\beta$ they can be used in conjunction with (23)–(25) to deduce that $b_{nn} = b_{n\phi} = 0$ and $b_{\phi\phi}/N_{4,0} = 7\zeta(3)/2\pi^2$, in the low temperature limit.

At zero doping, all three coefficients have essentially the same value, and from the

preceding paragraph we understand why $b_{\phi\phi}$ remains nearly constant up to very large doping, whereas b_{nn} and $b_{n\phi}$ drop quite sharply. In fact, they reach *negative* values for intermediate dopings. For these dopings, the truncation to fourth order in the fields gives a potential which is unbounded from below. Thus the expansion of the potential cannot be used to determine the minimum in the n direction, and our goal of finding the absolute minimum cannot be attained by expanding only to quartic order. We must use the full functional form of the free energy for this purpose.

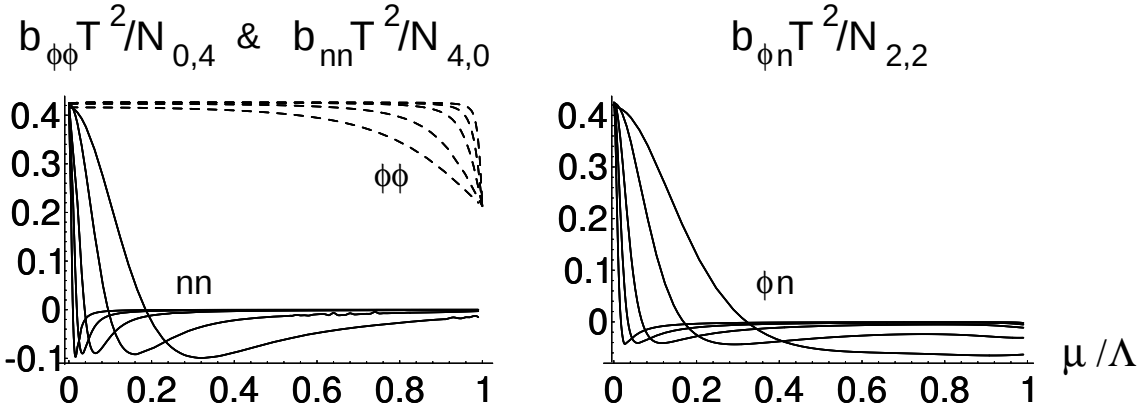

Figure 3

The coefficients $b_{\phi\phi}T^2/N_{0,4}$, $b_{nn}T^2/N_{4,0}$ and $b_{n\phi}T^2/N_{2,2}$ as a function of μ/Λ, for Λ/T=10, 20, 50, 100 and 200. The curves approach an asymptotic limit as $\Lambda/T\to\infty$.

4.4) Numerical Results for Arbitrary ϕ and n

In computing the full expression for F_1 in eq. (14), we can no longer factorize the momentum integral into a product of the form $\int d^{d-1}k\, G(k) \int d\varepsilon H(\varepsilon)$ because the integrand is not a simple polynomial in f_p and g_p. However we can still treat it similarly to our previous computations if we consider the special case where f^2 and g^2 are constant. We do not expect this assumption to radically change the features of the more general case, since the k-dependence of f and g has played no essential role in the preceding discussion. Constant g^2 still describes d-wave SC and is consistent with $SO(5)$ symmetry, so long as g changes sign across the nesting surface, *e.g.* $g_p = \mathrm{sign}(\varepsilon_p)$.

With this assumption, the free energy reduces to a single integral over the energy. We have evaluated it numerically for the relevant ranges of doping, temperature, and order parameters. The results are most conveniently expressed in terms of the following variables, for which the cutoff, Λ, is scaled out:

$$\hat{\phi} = g\phi/\Lambda; \quad \hat{n} = fn/\Lambda; \quad x = \mu/\Lambda; \tag{30}$$

$$\hat{a}_\phi = a^0_\phi/(4N_{0,0}g^2); \quad \hat{a}_n = a^0_n/(4N_{0,0}f^2); \quad \hat{\beta} = \beta\Lambda/2 \tag{31}$$

$$\hat{\varepsilon} = \varepsilon/\Lambda; \quad \hat{\lambda}_\pm = ((\sqrt{\hat{\varepsilon}^2 + \hat{n}^2} \pm x)^2 + \hat{\phi}^2)^{1/2}; \tag{32}$$

$$\Delta\hat{F} = \frac{1}{\hat{\beta}} \int_0^1 d\hat{\varepsilon} \ln \left(\frac{\cosh(\hat{\beta}\hat{\lambda}_+) \cosh(\hat{\beta}\hat{\lambda}_-)}{\cosh(\hat{\beta}(\hat{\varepsilon} + x)) \cosh(\hat{\beta}(\hat{\varepsilon} - x))} \right) \tag{33}$$

In the last line we subtracted a constant to make $\Delta\hat{F}$ vanish at $\phi = n = 0$. Then the full effective potential can be written in terms of

$$\hat{F} \equiv F/(4N_{0,0}\Lambda^2) = \hat{a}_\phi\hat{\phi}^2 + \hat{a}_n\hat{n}^2 + \Delta\hat{F}(\hat{\phi}, \hat{n}, \hat{\beta}, x). \tag{34}$$

In figure 4 we show $\hat{F}$ for six values of the doping parameter, $x = 0$, 0.2, 0.4, 0.6, 0.8 and 1 (horizontal rows), and along three directions in the ϕ-n plane (vertical columns). $\hat{F}$ is plotted as a function of $\hat{\phi}^2$, $(\hat{\phi}^2 + \hat{n}^2)/2$, and $\hat{n}^2$, in the three respective columns. Each graph is shown for the range of temperatures given by $\beta\Lambda = 4,\ 10,\ 20$, and 200, with $\hat{F}$ always increasing with temperature. We have chosen $\hat{a}_\phi = 2$ and $\hat{a}_\phi = 1.6$, hence $SO(5)$-breaking at the 20% level, in order to illustrate the phenomenologically desired dominance of the AF phase at low doping. At $x = 0$, the lowest minimum clearly occurs for $n \neq 0$. At $x = 0.2$, the minima become degenerate and the transition to the SC phase begins. Further increasing the doping quickly removes the AF instability, and gradually quenches the SC phase as well, depending on the temperature. This is in complete agreement with the picture obtained from our analysis of the quadratic coefficients and confirms the phase diagram shown in fig. 2.

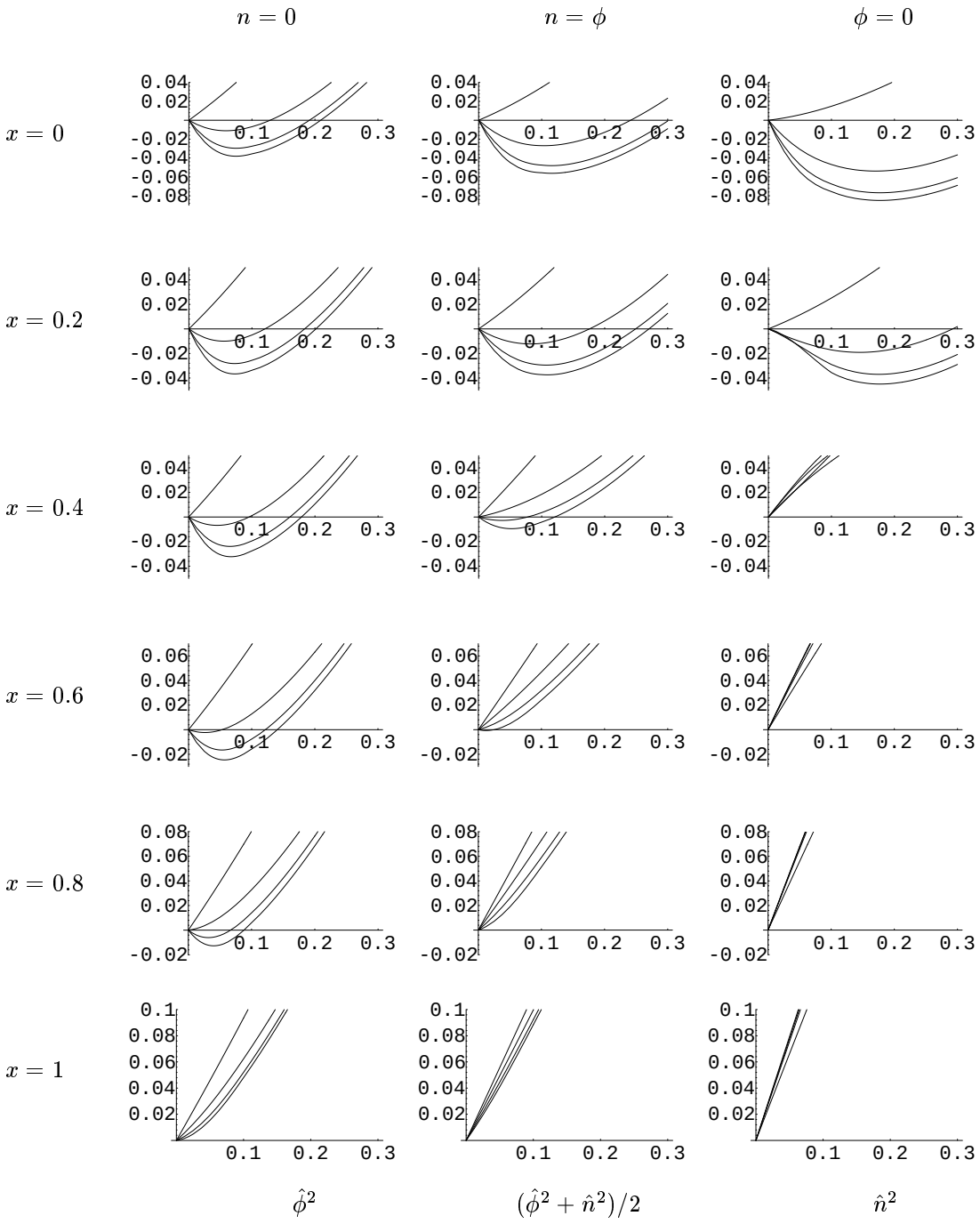

Figure 4

The rescaled effective potential $\hat{F}$ for six values of the doping parameter, x (horizontal rows) and along three directions in the ϕ-n plane (vertical columns). $\hat{F}$ is plotted as a function of $\hat{\phi}^2$, $\left(\hat{\phi}^2+\hat{n}^2\right)/2$, and $\hat{n}^2$, in the three respective columns. Each graph is shown for the range of temperatures given by $\beta\Lambda$=4, 10, 20, and 200, with $\hat{F}$ always increasing with temperature.

4.5) Terms with Derivatives

So far we have presented the one-loop free energy only for spatially constant order parameters. If $\phi(x)$ and $n(x)$ are not constant, there will be additional terms depending on their spatial derivatives. Of these, the most interesting are the $(\nabla\phi)^2$ and $(\nabla n)^2$ terms, since they are needed to compute quantum corrections coming from within the effective long-wavelength theory (two-loop and higher corrections).

By calculating the relevant Feynman diagrams, it is straightforward to show that the quadratic terms in F_1 for ϕ_q and n_q with an arbitrary momentum q can be obtained from our previous formulas (21)–(22) by making the replacements

$$T_\beta(\xi) \to \frac{\tanh(\beta\xi_{p+q/2}/2) + \tanh(\beta\xi_{p-q/2}/2)}{\xi_{p+q/2} + \xi_{p-q/2}}, \tag{35}$$

$$f(p,q) \to f(p-q/2,q), \qquad g(p,q) \to g(p-q/2,q), \tag{36}$$

where $\xi_p = \varepsilon_p - \mu$ and p is the loop momentum to be integrated over. Expanding in the external momentum $\vec{q}$ gives the expansion in derivatives of the fields. From this prescription it is clear that $SO(5)$ symmetry will be realized in the derivative terms so long as $f^2(p,q) = g^2(p,q)$ and $\mu = 0$, since the symmetry is then manifest in the energy eigenvalues $\lambda_\pm$ that appear in (15).

The resulting integral over p depends on the exact form of the dispersion relation ε_p and the coupling functions f_p, g_p, so we will defer further evaluation until the next section where we consider a specific choice of these functions.

5. Exact Results in a Specific Model

Our analysis so far has relied upon the approximation that the most important contributions to the effective potential are coming from electronic excitations near the Fermi surface. This approximation presupposes the Fermi energy to be much greater than the temperature and the chemical potential. On the other hand this hierarchy of scales may only be a factor of 10 in the actual cuprate systems we are interested in. It is therefore interesting to corroborate our conclusions without assuming that F_1 is dominated by

the contributions from near the FS. In this section we will exactly evaluate the first few terms in the small-field expansion of F using a semi-realistic lattice dispersion relation and pairing functions, which have been previously suggested in the literature [1,5,9]. It will be shown that the results are in good qualitative agreement with those based on the RG approach.

5.1) Method of Solution

For our specific model, we take the lattice dispersion relation (4) of the extended Hubbard model and choose

$$f(p,q) = 1, \qquad g(p-q/2,q) = (\cos(ap_x) - \cos(ap_y))/2 \tag{37}$$

as would be appropriate for s-wave AF pairing and d-wave SC pairing. The factor of 2 in the definition of g is chosen such as to maximize the $SO(5)$ symmetry near the undoped FS, as is shown below, and the q dependence is chosen to simplify the derivative terms to be computed at the end of this section. We further assume that the system is two dimensional, $d = 2$.

The choice (37) is motivated by two considerations: (1) we wish to examine to what extent $SO(5)$ symmetry survives when $f^2 \neq g^2$, since it has been suggested that $SO(5)$ can be a good approximate symmetry in the long-wavelength limit, even if it is not exact in the fundamental Hamiltonian; and (2) one would like to see how much the general features of the phase diagram depend on having exact $SO(5)$ symmetry in the Hamiltonian. We will show that making $f^2 \neq g^2$ breaks the symmetry significantly due to fluctuations far from the Fermi surface, even though those close to the FS give contributions to the free energy which are approximately $SO(5)$-symmetric. Nevertheless, the phase diagram is not affected in a qualitative way, and should still have the shape shown in figure 2.

The effective potential at $q = 0$ is still given by the general expression (14), but now the momentum integrals range over the Brillouin zone, $-\pi/a < p_x, p_y < \pi/a$, and there is no need to introduce any cutoff because the energy is explicitly bounded by $-4t < \varepsilon < 4t$.

As before, we expand F to quadratic and quartic order in the fields. Defining $\xi_p = \varepsilon_p - \mu$, this gives

$$F_1 = -\int \frac{d^2p}{(2\pi)^2}\left(2T_\beta(\xi_p)\left(|g_p\phi|^2 + n^2\frac{\xi_p}{\varepsilon_p}\right) + \frac{T'_\beta(\xi_p)}{2\xi_p}\left(|g_p\phi|^2 + n^2\frac{\xi_p}{\varepsilon_p}\right)^2 + \frac{\mu}{2\varepsilon_p^3}T_\beta(\xi_p)n^4\right). \tag{38}$$

Next one would like to reexpress the momentum integrals as an integral over the energy times an integral over the Fermi surface. This can be accomplished using the identity

$$\int d^2p\, g_p^m = \frac{4}{a^2}\int_{-4t}^{4t} d\varepsilon \int_{-1}^{1}\int_{-1}^{1} \frac{du\, dv\, (u-v)^m 2^{-m}}{\sqrt{1-u^2}\sqrt{1-v^2}}\delta(\varepsilon + 2t(u+v)), \tag{39}$$

where $u = \cos(ap_x)$ and $v = \cos(ap_y)$. The integrals over u and v can be done exactly, leaving an energy integral times a density of states function,

$$\int d^2p\, g_p^m = \frac{4}{a^2 t}\int_{-4t}^{4t} d\varepsilon\, \mathcal{N}_m(\varepsilon/4t). \tag{40}$$

The density of states $\mathcal{N}_m$ is given in terms of complete elliptic functions K and E; [5] defining $\hat{\varepsilon} = \varepsilon/4t$ and $\alpha = (1+|\hat{\varepsilon}|)/(1-|\hat{\varepsilon}|)$, the first few are

$$\mathcal{N}_0(\hat{\varepsilon}) = \frac{1}{1+|\hat{\varepsilon}|}K(1/\alpha) \tag{41}$$

$$\mathcal{N}_2(\hat{\varepsilon}) = (1+|\hat{\varepsilon}|)\big(K(1/\alpha) - E(1/\alpha)\big) \tag{42}$$

$$\mathcal{N}_4(\hat{\varepsilon}) = \frac{1}{3}\alpha(1-|\hat{\varepsilon}|)^3\big((2\alpha^2+1)K(1/\alpha) - 2(\alpha^2+1)E(1/\alpha)\big) \tag{43}$$

These are shown in fig. 5. Because of our choice of normalization for g_p in (37), they all have the same asymptotic behavior near the undoped FS, $\varepsilon = 0$: $\mathcal{N}_m \sim \ln(1/|z|)$, independent of m. However they quickly diverge from each other for energies above or below the FS. This is interesting from the point of view of the $SO(5)$ symmetry, because it shows that even though $g^2 \neq 1$, as is necessary to have exact $SO(5)$, close to the FS the symmetry is nevertheless approximately realized. However the logarithmic singularity

[5] as they are defined in all standard mathematical references except for Abramovitz and Stegun and Mathematica, which use a nonstandard convention. See for example [10]

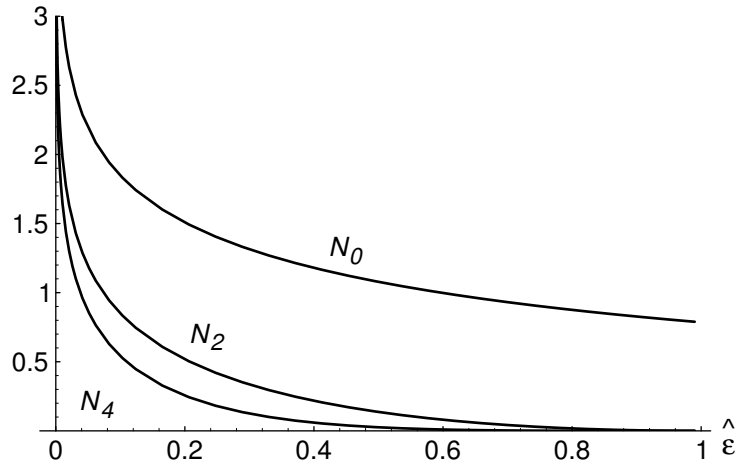

Figure 5

The density of states $\mathcal{N}_0$, $\mathcal{N}_2$ and $\mathcal{N}_4$ as a function of $\hat{\varepsilon} = \varepsilon/4t$.

near $\varepsilon = 0$ in $\mathcal{N}_m$ is too weak to compensate for the $SO(5)$-breaking differences between $\mathcal{N}_0$ and $\mathcal{N}_2$ away from the FS, as we will presently show.

5.2) Expansion near $\phi = n = 0$

Now the expressions for the coefficient functions in the small-field expansion of F_1 can be written in a way which looks very similar to our previous results (21)–(25). Let us first define

$$\kappa = \frac{4}{\hbar^2 (2\pi)^2 a^2 t} = \frac{2m}{(\pi\hbar)^2}, \tag{44}$$

where a is the lattice spacing, and m is the quasiparticle mass in the vicinity of the FS, where the dispersion relation can be approximated as $\varepsilon = p^2/2m$. We then obtain

$$a_\phi = a_\phi^0 - \kappa \int_{-4t}^{4t} d\varepsilon \; T_\beta(\xi)\, \mathcal{N}_2(\varepsilon/4t) \tag{45}$$

$$a_n = a_n^0 - \kappa \int_{-4t}^{4t} d\varepsilon \; T_\beta(\xi) \frac{\xi}{\varepsilon} \mathcal{N}_0(\varepsilon/4t), \tag{46}$$

$$b_{\phi\phi} = -\kappa \int_{-4t}^{4t} d\varepsilon \, \frac{T_\beta'(\xi)}{\xi} \mathcal{N}_4(\varepsilon/4t), \tag{47}$$

$$b_{\phi n} = -\kappa \int_{-4t}^{4t} d\varepsilon \, \frac{T'_\beta(\xi)}{\varepsilon} \mathcal{N}_2(\varepsilon/4t), \tag{48}$$

$$b_{nn} = -\kappa \int_{-4t}^{4t} d\varepsilon \, \left(\frac{T'_\beta(\xi)}{\varepsilon} - \frac{\mu}{\varepsilon} \frac{\partial}{\partial \varepsilon} \left(\frac{T_\beta(\xi)}{\varepsilon} \right) \right) \mathcal{N}_0(\varepsilon/4t). \tag{49}$$

The dependence of these coefficients on doping and temperature is shown in Figures 6 and 7, which can be compared to Figures 1 and 3 from our model-independent analysis. In Figure 6, which shows the 1-loop contributions to the quadratic coefficients, one sees that our previous result for a_n is in good agreement with the exact computation in the present model. This is not suprising because f_p is treated as a constant in both cases, and the only difference between the two is the lattice dispersion relation in the present computation versus the approximation $\varepsilon \approx v_{\scriptscriptstyle F} \ell$ in §4. However the difference between the two approaches is quite apparent in a_ϕ, where g_p is relevant: a_ϕ increases with doping faster in the exact computation than in the approximation of factoring out the FS integration. Nevertheless the important qualitative feature needed to obtain the phase diagram of Figure 2 persists: a_ϕ increases more slowly as a function of doping than does a_n.

Similar remarks apply in comparing the quartic coefficients in the two treatments. The difference in the dispersion relation causes a small change in the T- and μ-dependence of b_{nn}, the coefficient that does not depend at all on g_p. Nevertheless in both analyses, b_{nn} and $b_{n\phi}$ have the same behavior of initially falling very sharply from positive to negative values as the chemical potential μ is increased from $\mu = 0$, and gradually becoming zero as $\mu \to 4t$. $b_{\phi\phi}$ falls much faster with x in the exact computation than in the previous one, but still more gradually than b_{nn} or $b_{n\phi}$. Again, this can be understood analytically in the low-temperature limit using (28)–(29), which gives $b_{nn} = b_{n\phi} = 0$ and $b_{\phi\phi} = (7\zeta(3)\beta^2 m/\pi^4\hbar^2)\mathcal{N}_4(\mu/4t)$ for $\mu \gg 1/\beta$. The qualitative agreement between the two approaches gives us confidence that the shape of the phase diagram in Figure 2 is indeed a robust prediction of the model, in the one-loop approximation.

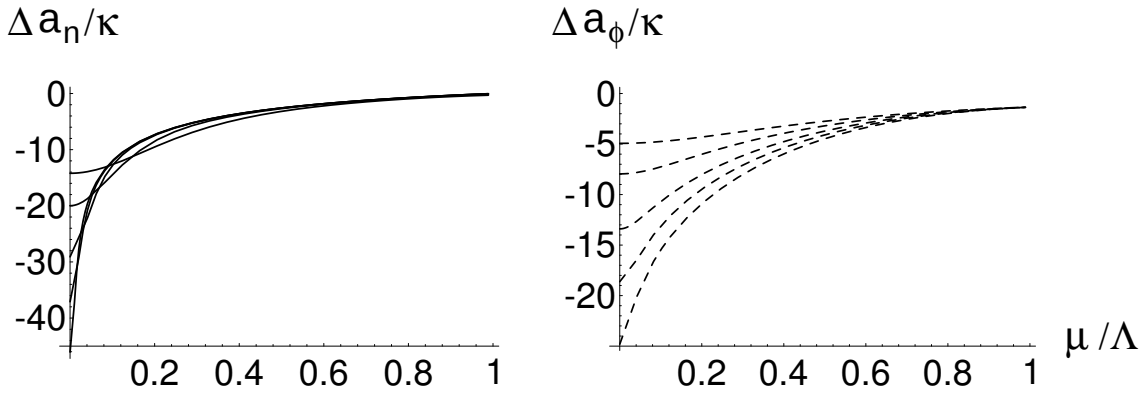

Figure 6

The exactly computed coefficients $(a_n - a_n^0)/\kappa$ (solid) and $(a_\phi - a_\phi^0)/\kappa$ (dashed) as a function of μ/Λ, for the same values of $\beta\Lambda$ as in Figures 1 and 3.

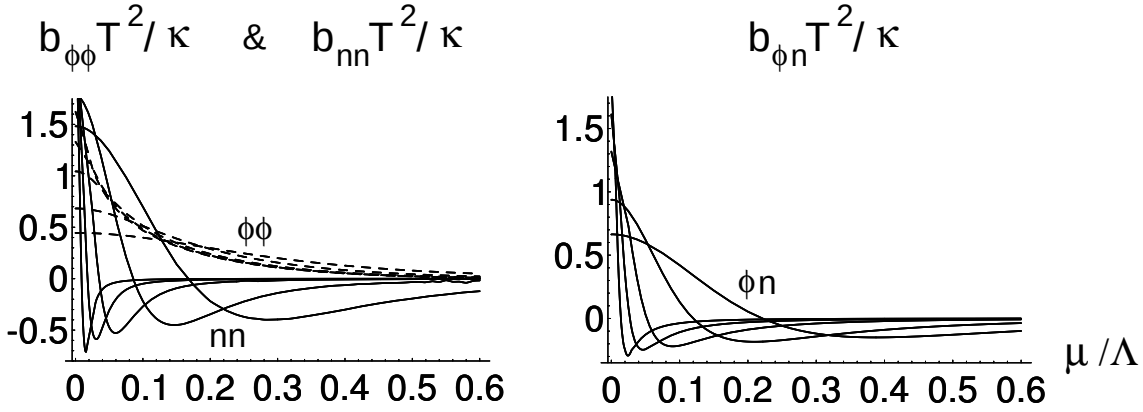

Figure 7

The exactly computed coefficients $b_{nn}T^2/\kappa$, $b_{n\phi}T^2/\kappa$ and $b_{\phi\phi}T^2/\kappa$ as a function of μ/Λ, for the same values of $\beta\Lambda$ as in Figures 1, 3 and 6.

5.3) $SO(5)$-breaking due to $g_p^2 \neq f_p^2$

One interesting issue we can explore within the exact computation is the extent to which $SO(5)$ symmetry is broken by the assumption of d-wave SC pairing versus s-wave AF pairing. In Fig. 6 one sees that, despite our tuning the normalization of g_p so as to preserve $SO(5)$ near the FS, $|\Delta a_n| > |\Delta a_\phi|$ even at zero doping. We could have tuned g_p such as to force $\Delta a_n = \Delta a_\phi$ at some temperature T_0, but the equality would hold only for

$T = T_0$. In fact we find that the ratio $\Delta a_\phi / \Delta a_n$ scales linearly with $\ln(\beta/4t)$:

$$\left(\frac{\Delta a_\phi}{\Delta a_n}\right)_{\mu=0} \cong 0.20 + 0.064\, \ln(\beta/4t). \tag{50}$$

For comparison, the breaking in the quartic couplings can be similarly parameterized in terms of the ratios

$$\left(\frac{b_{\phi\phi}}{b_{nn}}\right)_{\mu=0} \cong 0.082 + 0.10\, \ln(\beta/4t); \qquad \left(\frac{b_{n\phi}}{b_{nn}}\right)_{\mu=0} \cong 0.27 + 0.084\, \ln(\beta/4t). \tag{51}$$

5.4) Derivative Terms in the Free Energy

Using the above techniques and the procedure discussed in §4.5, we can evaluate the lowest derivative terms in the quadratic part of F_1,

$$F_1 = c_\phi (\nabla\phi)^2 + c_n (\nabla n)^2. \tag{52}$$

Defining $\kappa' = \beta^2 t/(4\pi\hbar)^2$, $\hat{\varepsilon} = \varepsilon/4t$, $\hat{\mu} = \mu/4t$, and going to the limit of large βt, we can write the coefficients as

$$c_\phi \cong \kappa' \int_{-4t}^{4t} d\varepsilon\, \frac{T_\beta(\xi)}{\cosh^2(\beta\xi/2)} \Big(\big(1-\hat{\varepsilon}^2\big)\, \mathcal{N}_2(\hat{\varepsilon}) - \big(1-|\hat{\varepsilon}|\big)^2\, \mathcal{N}_4(\hat{\varepsilon}) \Big) \tag{53}$$

$$\cong \frac{14\zeta(3)\kappa'}{\pi^2} \Big(\big(1-\hat{\mu}^2\big)\, \mathcal{N}_0(\hat{\mu}) - \big(1-|\hat{\mu}|\big)^2\, \mathcal{N}_2(\hat{\mu}) \Big)\,; \tag{54}$$

$$c_n \cong \kappa' \int_{-4t}^{4t} d\varepsilon\, \frac{T_\beta(\xi)}{\cosh^2(\beta\xi/2)} \left(\frac{\xi}{\varepsilon}\right) \Big(\big(1-\hat{\varepsilon}^2\big)\, \mathcal{N}_0(\hat{\varepsilon}) - \big(1-|\hat{\varepsilon}|\big)^2\, \mathcal{N}_2(\hat{\varepsilon}) \Big) \tag{55}$$

$$\sim O(1/\beta t)\, c_\phi \tag{56}$$

To obtain (54) we used the identity (28), which is however only valid for $\mu \gg 1/\beta$. For $\mu \lesssim 1/\beta$, the logarithmic singularities in $\mathcal{N}_0$ and $\mathcal{N}_2$ are integrated over to obtain result that is finite as $\mu \to 0$. The identity (28) gives a vanishing result when applied to (55), meaning that c_n is of order $1/\beta t$ compared to c_ϕ, and thus c_n must be computed numerically to find

the leading behavior in the large βt limit. Again, these statements hold only for $\mu \gg 1/\beta$ due to the singular behavior of the integrand at $\varepsilon = 0$. For $\mu \lesssim 1/\beta$, we expect that $c_\phi \sim c_n$, just as was found for the coefficients of the quartic terms.

These derivative terms will not be of further use in the present preliminary study, but may be useful in computing the higher order quantum corrections which we leave for future investigation.

6. Conclusions

In summary, our calculations lead us to the following conclusions:

• *Microscopic $SO(5)$ Invariance:* We find, by construction, that microscopic models can indeed give rise to $SO(5)$ invariance which relates the d-wave superconducting and antiferromagnetic phases. This symmetry can emerge accidentally at long wavelengths, and so be relevant for the effective potential which determines which phase is energetically preferred (in a homogeneous system). Being a long-wavelength effect, the symmetry can be easily hidden in treatments which include all scales together.

• *Features of the Phase Diagram:* Using our model we have computed the Landau-Ginzburg free energy whose minimization determines the phase diagram in the temperature-doping plane. We find that the coefficients of the Landau-Ginzburg potential have the right qualitative dependence on temperature and chemical potential to allow for antiferromagnetism at half filling, but which is destroyed as the system is doped. It can also describe a superconductor which is favoured only for a range of nonzero dopings.

• *Significance of the $SO(5)$ Symmetry:* The class of models we considered encompasses $SO(5)$ symmetry as a special case among the most general possible coupling functions. We find that if the symmetry is broken in the microscopic theory, there is no special tendency for it to be restored or further broken in the effective long-wavelength theory. The phase diagram is only of the desired form if there is a certain level of $SO(5)$-breaking, whose fundamental origin is unknown. In the specific model considered in §5, the symmetry appears to be badly broken, since f_p^2 and g_p^2 are quite different functions of momentum,

yet by tuning their relative sizes it appears possible to obtain the correct phase diagram. At present it is therefore not yet clear whether nature demands an approximate $SO(5)$ symmetry as the correct way to understand the relation between the AF and SC phases in cuprates, or whether $SO(5)$-symmetric models simply fall into the same universality class as the correct theory.

Acknowledgments

We thank the organizers and participants of the Benasque Centre for Physics, for providing such a pleasant and stimulating setting for part of this work. We thank P.K. Panigrahi for useful discussions, and C.A. Lütken for collaborations in early stages of this work. Our research was partially funded by the N.S.E.R.C. of Canada and by the Fonds F.C.A.R. du Québec.

7. References

[1] S.-C. Zhang, Science **275** (1997) 1089.

[2] M. Greiter, preprints cond-mat/9705049, cond-mat/9705282.

[3] S.C. Zhang, preprint cond-mat/9705191.

[4] G. Baskaran and P.W. Anderson, preprint cond-mat/9706076.

[5] S. Rabello, H. Kohno, E. Demler and S.C. Zhang, preprint cond-mat/9707027.

[6] C.P. Burgess and C.A. Lütken, preprints cond-mat/9611070; cond-mat/9705216.

[7] J. Polchinski, *Effective Field Theory of the Fermi Surface*, in *Recent Developments in Particle Theory, Proceedings of the 1992 TASI*, eds. J. Harvey and J. Polchinski (World Scientific, Singapore, 1993);

R. Shankar, *Renormalization Group Approach to Interacting fermions*, *Rev. Mod. Phys.* **66** (1994) 129;

T. Chen, J. Fröhlich and M. Seifert, *Renormalization Group Methods: Landau-Fermi Liquid and BCS Superconductor*, preprint cond-mat/9508063.

[8] P.-C. Dai, H.A. Mook and F. Dogan, cond-mat/9707112.

[9] D.L. Feder and C. Kallin, *Phys. Rev.* **B** (1997) , cond-mat/9609248;

S. Stintzing and W. Zwerger, *Phys. Rev.* **B** (1997) , cond-mat/9703129.

[10] I.S. Gradshteyn and I.M. Ryzhik, Table of Integrals, Series and Products (Academic Press, New York, 1980)